Available online at www.sciencedirect.com

ScienceDirect

ARTICLE

Hot Deformation Behavior and Processing Maps of As-Homogenized Mg-Gd-Y-Zn-Mn Alloy

Wang Jingfeng[1,2], Xie Feizhou[1], Liu Shijie[1], Huang Song[1], Pan Fusheng[1]

[1] National Engineering Research Center for Magnesium Alloys, Chongqing University, Chongqing 400044, China; [2] State Key Laboratory of Mechanical Transmission, Chongqing 400044, China

Abstract: The hot deformation behavior and processing maps of as-homogenized Mg-Gd-Y-Zn-Mn alloy were investigated by hot compression tests performed at 350~500 °C and strain rates ranging from 0.001 s^{-1} to 1 s^{-1}. The constitutive equation was established using hyperbolic law, and the activation energy of the alloy was calculated to be about 260.94 kJ/mol. Based on the dynamic material model, processing maps of as-homogenized Mg-Gd-Y-Zn-Mn alloy deformed at strain values of 0.6, 1.2 were drawn to study the hot workability of the alloy. The processing map developed at a strain of 1.2 shows two safety domains: one occurring at 460~500 °C and strain rates ranging from 0.001 s^{-1} to 1 s^{-1}; the other occurring at 350~500 °C, and strain rate ranging from 0.001 s^{-1} to 0.005 s^{-1}. The corresponding microstructure evolution, with particular emphasis on the deformation mechanism of long-period stacking ordered phase (LPSO) in this alloy, was also discussed.

Key words: Mg-Gd-Y-Zn-Mn alloy; hot deformation; processing map; optimum processing parameter; microstructure

Given their high strength and creep resistance, wrought magnesium alloys containing the rare-earth (RE) elements Gd and/or Y have great potential structural applications in the aerospace, railway, and automotive industries[1]. In contrast to conventional magnesium alloys, the magnesium alloys containing RE elements are subjected to plastic deformation such as extrusion, rolling, and forging possess fine-grained strengthening effect and show superior mechanical properties. However, difficulties are encountered in deforming these magnesium alloys into components owing to their HCP crystal structure with limited slip systems.

Processing maps based on the dynamic material model (DMM) is a very useful tool for optimizing hot processing parameters and is widely used to understand the hot workability of many materials, especially those that are hard to deform[2-4]. In the previous studies, H. Z. Li et al.[5] investigated the hot deformation behavior and processing maps of as-cast Mg-10Gd-4.8Y-2Zn-0.6Zr alloy. The optimum parameters for the hot working of the alloy were the deformation temperature of 500 °C and strain rate of 0.01 s^{-1}. However, microstructure analysis reveals only a simple description of recrystallization rather than a systematic study on the important second-phase LPSO in this alloy during hot deformations. N. Tahreen et al.[6] studied the hot behavior of as-extruded ZM31+6Y alloy, with particular emphasis on the mechanisms of LPSO phase. Kink bands, which are involved in an essential deformation mechanism, have been observed by the motion of dislocation pairs.

As a kind of high-strength magnesium alloys, Mg-Gd-Y-Zn alloys typically consist of both MgGdZn and MgZnY LPSO phases[7]. In the present study, Mn was added because Mn can refine the grains of as-cast alloys and restrict the growth of recrystallization grains during hot deformations[8]. Mn can also reduce the difficulties during the metallurgical process to a certain extent.

Our previous study has shown that Mg-8.4Gd-5.3Y-1.6Zn -0.6Mn alloy can achieve 500 MPa with an elongation of 10% by extrusion and subsequent aging[9]. However, to the author's

Received date: June 16, 2017
Foundation item: National Natural Science Foundation of China (51571044); National Key Research and Development Program of China (2016YFB0301102); Chongqing Foundation and Advanced Research Project (cstc2015jcyjBX0081)
Corresponding author: Wang Jingfeng, Ph. D., Professor, College of Materials Science and Engineering, Chongqing University, Chongqing 400044, P. R. China, Tel: 0086-23-65112153, E-mail: jfwang@cqu.edu.cn

knowledge, little is known about the forging or rolling of Mg-Gd-Y-Zn-Mn alloy, which is also a significant process in industry production. Before these processes, the deformation simulation of this alloy through thermal simulation test data is necessary.

In the present study, the hot deformation behavior of as-homogenized Mg-Gd-Y-Zn-Mn alloy based on simulation tests was investigated, and processing maps were drawn. The goals were to understand the characterization of dynamic recrystallization (DRX) under different processing conditions and optimize the hot working parameters of this alloy during hot processing, such as forging and rolling. At the same time, the deformation mechanism of both MgGdZn and MgZnY LPSO phases was also discussed in detail.

1 Experiment

Experiments were carried out on Mg-8.7Gd-3.7Y-1.4Zn-1Mn alloy, which was produced by semi continuous casting. The as-cast ingot was homogenized at 540 °C for 4 h and cooled in a furnace. The cylindrical specimens with the dimensions of Φ12 mm×8 mm were cut from the as-homogenized ingot. Uniaxial compression tests were conducted at true strain rates of 0.001, 0.01, 0.1, and 1 s^{-1} and temperatures of 350, 400, 450, and 500 °C on a Gleeble-1500 thermo-mechanical simulator.

Before the compression tests, the surface of samples was polished. To reduce the deformation friction, a graphite lubricant was needed between the sample and crosshead. The samples were first heated to the deformation temperature at a heating rate of 10°C /s and held for 60 s to obtain a stable and uniform microstructure, and then deformed up to the total true strain of 1.2. To freeze the deformed microstructures for optical observation, all samples were quenched in water less than 5 s after compression.

Optical microscopy was used to examine the microstructure of deformed samples, which were sectioned in the center parallel to the compression axis. To analyze the microstructure, a scanning electron microscopy (SEM) system was used. The etching solution was 4 vol% HNO_3 with ethanol.

2 Results and Discussion

2.1 Microstructures of as-cast and as-homogenized samples

The optical micrograph of as-cast Mg-Gd-Y-Zn-Mn alloy, which has coarse grains and a network of secondary phase, is shown in Fig.1a. The optical micrograph after homogenization is shown in Fig.1b. SEM was used to obtain more information about the microstructure before and after homogenization. Before hot treatment, the as-cast sample exhibits a microstructure consisting of α-Mg, white eutectic phase, and gray LPSO phase, as shown in Fig.1c. The secondary phase crystallizes at the grain boundaries. After treatment, two kinds of morphology of LPSO phases are observed, as shown in Fig.1d. One is the original gray bulk phase, and the others are the lamellar phases that precipitated in the grain of this alloy. The white eutectic phases disappeared because of the high solid solubility of the RE elements in magnesium, but the gray LPSO phases do not disappear because they are stable structures[10].

2.2 Flow stress behavior

The typical true stress-true strain curves of as-homogenized Mg-Gd-Y-Zn-Mn alloy obtained from compression tests deformed up to a true strain of 1.2 at 350~500 °C and strain rate ranging from 0.001 s^{-1} to 1 s^{-1} are shown in Fig.2. The

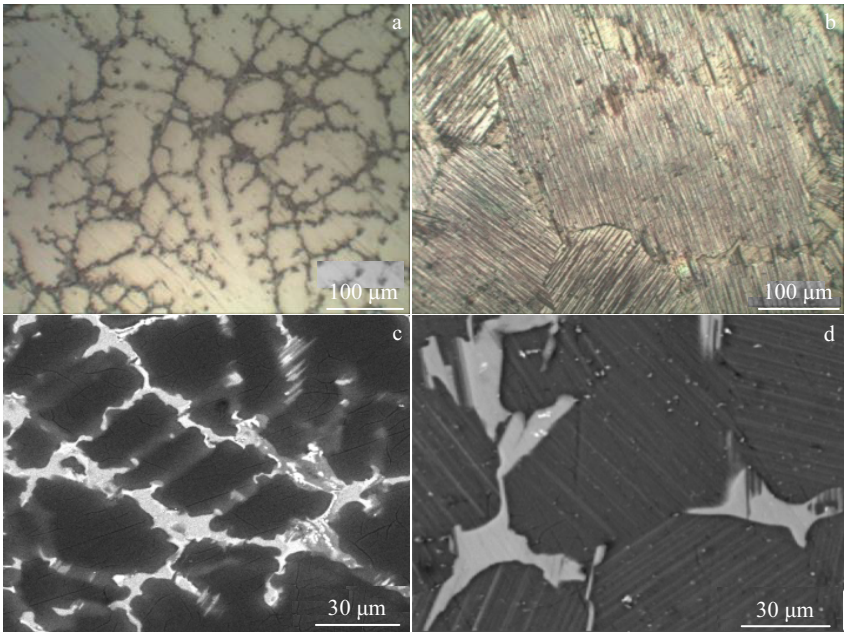

Fig.1 Optical micrographs (a, b) and SEM images (c, d) of the Mg-Gd-Y-Zn-Mn alloys before (a, c) and after (b, d) the homogenizing treatment

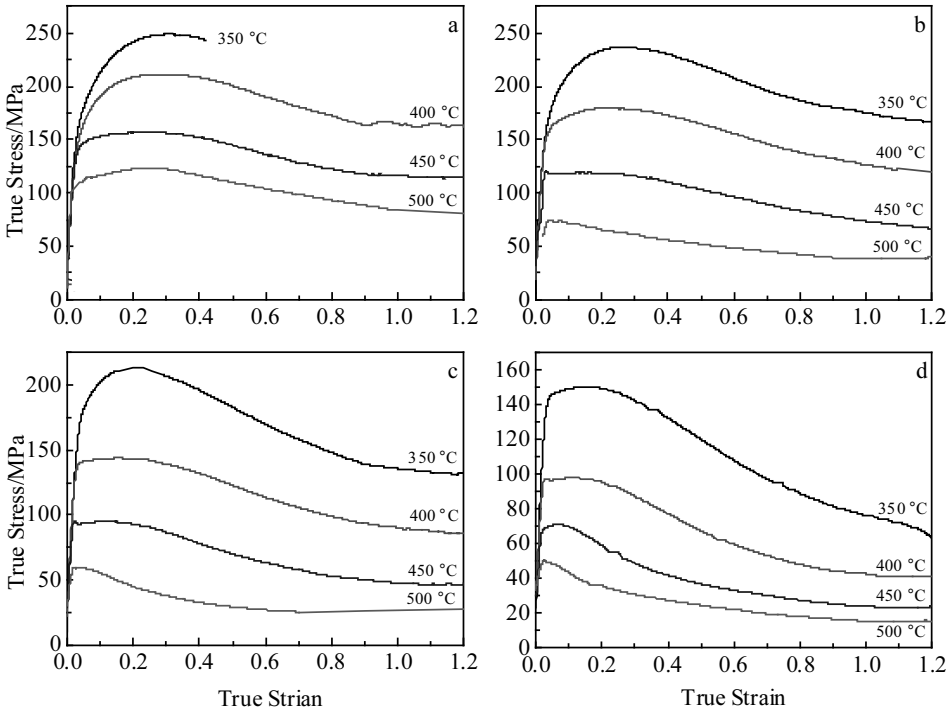

Fig.2 True stress-true strain curves of the alloy during the hot compression: (a) 1 s^{-1}, (b) 0.1 s^{-1}, (c) 0.01 s^{-1}, and (d) 0.001 s^{-1}

general features of the flow stress curves are similar under almost all deformation conditions. Hot deformation is a competition of work hardening by dislocation storage and work softening by the dynamic recrystallization (DRX) or recovery. At the beginning, flow stress increases sharply to a maximum because work hardening exceeds the work softening with the dislocation density increasing largely. As the compression continues, flow stress decreases to a steady state because work softening compensates or partially compensates for the effect of work hardening. In particular, differences in the deformation behavior of the curves could be observed. At low temperatures (350 and 400 °C), the alloy exhibits greater work hardening followed by substantial work softening. At 350 °C and strain rate of 1 s^{-1}, the shear fracture even occurs compressed to the true stain of 0.4. Conversely, at higher temperature (450 and 500 °C), the material displays less obvious work hardening followed by mild work softening, leading to a steady state.

The peak flow stress is known to depend on the compression temperature and strain rate. At a given temperature, flow stress increases with increased strain rate because time is insufficient for energy accumulation and dislocation annihilation at high strain rate. For instance, peak stress changes from 50 MPa to 125 MPa with increased strain rate from 0.001 s^{-1} to 1 s^{-1} at 500 °C. Meanwhile, due to the movement of the dislocation enhanced by the augmented thermal activation of the alloy, at a given strain rate, flow stress is lower when compression temperature is higher. As it can be clearly seen in Fig.2d, the peak stress decreases from 150 MPa to 50 MPa with increased temperature from 350 °C to 500 °C at a strain rate of 0.001 s^{-1}.

2.3 Kinetic analysis

The thermally activated process is one of the main characteristics of deformation mechanisms in hot deformation. At various stress levels, the relationship of strain rate with flow stress and temperature can be described by the Arrhenius equation in the following three ways. At low stress level, the power law (Eq. (1)) is suitable, and at high stress level, the relationship can be described by exponential law (Eq.(2)); the hyperbolic law (Eq. (3)) has been widely used to describe the relationship at all the stress levels:

$$\dot{\varepsilon} = A_1\sigma^{n_1}\exp(-\frac{Q}{RT}) \qquad (\alpha\sigma<0.8) \tag{1}$$

$$\dot{\varepsilon} = A_2\exp(\beta\sigma)\exp(-\frac{Q}{RT}) \qquad (\alpha\sigma>1.2) \tag{2}$$

$$\dot{\varepsilon} = A[\sinh(\alpha\sigma)]^n\exp(-\frac{Q}{RT}) \tag{3}$$

By changing the form of Eq. (3), we obtain

$$Z = \dot{\varepsilon}\exp(\frac{Q}{RT}) = A[\sinh(\alpha\sigma)]^n \tag{4}$$

where $\dot{\varepsilon}$ is the strain rate, σ is the flow stress, Q is the effective activation energy of deformation (kJ/mol), and T is the absolute temperature. Moreover, A, A_1, A_2, n, n_1, α, and β are the constants of the materials ($\alpha = \beta/n_1$), and R is the gas constant (8.314 $J\cdot mol^{-1}\cdot K^{-1}$). Z refers to the Zener-Hollomon

parameter, which can be used to describe the combined effects of temperature and strain rate on hot deformation.

For better understanding, we can rewrite Eqs. (1) and (2) as

$$\ln\sigma = \frac{\ln\dot{\varepsilon}}{n_1} - \frac{\ln A_1}{n_1} + \frac{Q}{n_1 RT} \quad (5)$$

$$\sigma = \frac{\ln\dot{\varepsilon}}{\beta} - \frac{\ln A_2}{\beta} + \frac{Q}{\beta RT} \quad (6)$$

Based on the equations above, flow stress is plotted against strain rate at different temperatures shown in Fig.3.

We can rewrite Eqs. (3) and (4) as:

$$\ln\dot{\varepsilon} = \ln A + n\ln[\sinh(\alpha\sigma)] - \frac{Q}{RT} \quad (7)$$

$$\ln Z = \ln A + n\ln[\sinh(\alpha\sigma)] \quad (8)$$

From Eq. (7), the value of Q at a certain rate could be calculated as follows

$$Q = R\left\{\frac{\partial\ln\dot{\varepsilon}}{\partial\ln[\sinh(\alpha\sigma)]}\right\}_T \left\{\frac{\partial\ln[\sinh(\alpha\sigma)]}{\partial(1/T)}\right\}_{\dot{\varepsilon}} \quad (9)$$

In this equation, $\left\{\frac{\partial\ln\dot{\varepsilon}}{\partial\ln[\sinh(\alpha\sigma)]}\right\}_T$ refers to the slope of $\ln\dot{\varepsilon}$-$\ln[\sinh(\alpha\sigma)]$ at various deformation temperatures, as shown in Fig.4a. Moreover, $\left\{\frac{\partial\ln[\sinh(\alpha\sigma)]}{\partial(1/T)}\right\}_{\dot{\varepsilon}}$ stands for the slope of $\ln[\sinh(\alpha\sigma)]$-$1/T$, as shown in Fig.4b.

Substituting the average value of the slope of $\ln\dot{\varepsilon}$-$\ln[\sinh(\alpha\sigma)]$ and $\ln[\sinh(\alpha\sigma)]$-$1/T$ into Eq.(9), the average value of

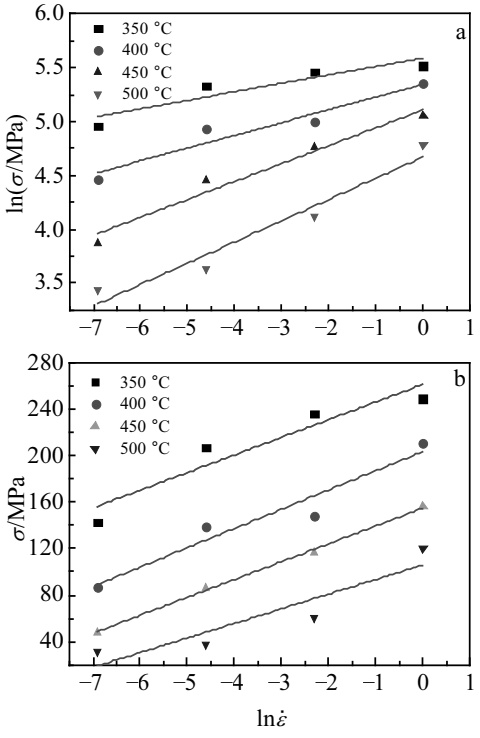

Fig.3 Relationship between $\ln\dot{\varepsilon}$ and $\ln\sigma$ (a) and σ (b)

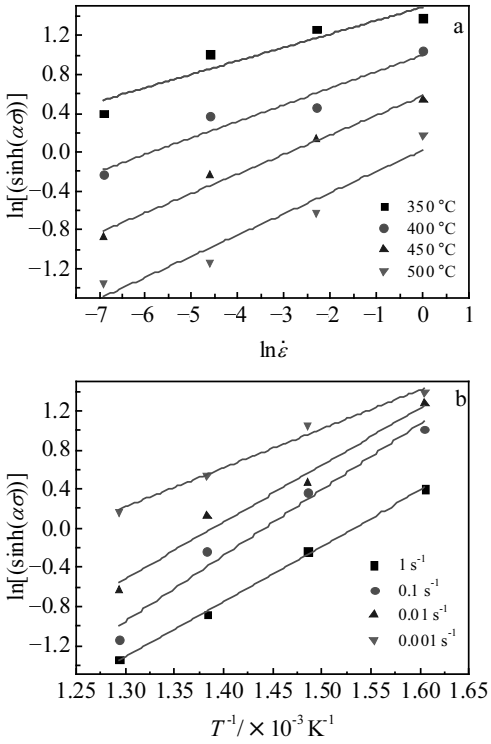

Fig.4 Relationship of $\ln[\sinh(\alpha\sigma)]$ to $\ln\dot{\varepsilon}$ (a) and $1/T$ (b)

deformation activation energy (Q) is 260.94 kJ/mol. The plastic deformation of a metal is a thermal activation process, during which atoms move quickly. To be motivated, atoms should reach the threshold called activation energy. Therefore, Q is a significant parameter that indicates deformation difficulty degree in hot deformation. Q is influenced by different factors, such as concurrent dynamic precipitation[11], dislocation pinning effect[12], and the second phase. The Q of as-cast Mg-Zn-Y-Zr alloy containing W-phase was determined to be 209 kJ/mol by Chen et al.[13]. Kwak et al.[14] obtained a Q of 176.3 kJ/mol for Mg-9.5Zn-2.0Y alloy with icosahedral quasicrystalline phase. These values are higher than that (135 kJ/mol) in pure magnesium. In the present work, the activation energy of as-homogenized Mg-Gd-Y-Zn-Mn alloy is estimated to be 260.94 kJ/mol. Obviously, Q increases chiefly because of the presence of the thermally stable LPSO phase, which could be huge barriers to the motion of dislocation.

Based on Eq.(8), ln$Z$ and $\ln[\sinh(\alpha\sigma)]$ should show the linear relationship. The relationship between the peak stress and the Zener-Hollomon parameter is shown in Fig.5. It can be concluded that the linear variation on $\ln[\sinh(\alpha\sigma)]$ with lnZ obtained by

$$\ln Z = 41.02354 + 5.40314\ln[\sinh(\alpha\sigma)] \quad (10)$$

Compared with Eq. (8), we know that ln$A$=41.023 54 and n=5.403 14. In the end, the values of A, n, α, and Q can be obtained. Substituting them into Eq.(3), the constitution equation can be expressed as

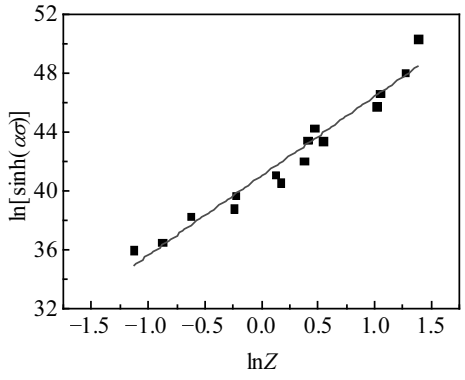

Fig.5 Relationship between Zener-Hollomon parameter and peak stress

$$\dot{\varepsilon} = 6.55\times10^{17}[\sinh(0.008376\sigma)]^{5.40314}\exp(-\frac{260.94}{8.314T}) \quad (11)$$

2.4 Processing maps and microstructure evolution

According to the DMM established by Prasad and co-workers[15], the deformation workpiece can be generally viewed as a power dissipater (*P*), which consists of two parts, namely, *G* content and *J* co-content. The former stands for power dissipation through plastic deformation, and the latter represents dissipation during the metallurgical process including DRX, dynamic recovery, or damage of materials.

G and *J* can be related by the strain-rate sensitivity parameter *m*, as shown below:

$$m = (\frac{\partial J}{\partial G})_{\varepsilon,T} = \frac{\partial J\partial P}{\partial P\partial G} = \frac{\sigma \mathrm{d}\dot{\varepsilon}}{\varepsilon \mathrm{d}\dot{\sigma}} = \left[\frac{\partial(\ln\sigma)}{\partial(\ln\dot{\varepsilon})}\right]_{\varepsilon,T} \quad (12)$$

At a given temperature and strain, the co-content *J* can be expressed as follows:

$$J = \int_0^{\sigma}\dot{\varepsilon}\mathrm{d}\sigma = \sigma\dot{\varepsilon}\cdot\frac{m}{m+1} \quad (13)$$

where $\dot{\varepsilon}$ is strain rate, and σ is flow stress. For the ideal linear dissipating body, *m*=1, so

$$J = J_{\max} = \frac{\sigma\dot{\varepsilon}}{2} \quad (14)$$

Therefore, the efficiency of power dissipation can be expressed as:

$$\eta = \frac{J}{J_{\max}} = \frac{2m}{m+1} \quad (15)$$

where η stands for power dissipation and varies with the change in strain rate and the flow stress. Based on the extremum principles of irreversible thermodynamics applied for a large plastic flowbody, an instability criterion is used to identify the regimes of flow instabilities, which is given by[16]:

$$\xi(\dot{\varepsilon}) = \frac{\partial\ln[m/(1+m)]}{\partial\ln\dot{\varepsilon}} + m \le 0 \quad (16)$$

where $\xi(\dot{\varepsilon})$ is the instability parameter. Under a certain deformation condition ($\xi(\dot{\varepsilon})$ is negative), flow instabilities occur because of shear band, flow localization, crack, dynamic strain aging, mechanical twinning, and kinking[17]. Therefore, a processing map can be drawn by overlapping the instability and the power dissipation map. Clearly, a processing map is useful for identifying the optimum deformation conditions and the flow instability domain.

The processing maps of as-homogenized Mg-Gd-Y-Zn-Mn alloy deformed at strains of 0.6 and 1.2 are shown in Fig.6, in which the counters represent the constant efficiency of power dissipation, and the shaded domain represents the unstable region. In Fig.6a, the maximum power dissipation coefficient is 0.44 when the deformation temperature range is 410~430 °C and the strain rate is 0.001 s^{-1}. In Fig.6b, the maximum power dissipation coefficient is 0.48 when the deformation temperature range is 370~410 °C and the strain rate is 0.001 s^{-1}. We think that the lower temperature with higher power dissipation maybe due to the effect of LPSO phase. At the same temperature and the same strain rate, with the increase of strain, the power dissipation coefficient increases. It is observed that as the strain increases the power dissipation map changes a little. In other words, strain level shows no obvious effect on the power dissipation map. The deformation mechanism and microstructure evolution were studied in detail on the processing map at a strain of 1.2.

Fig.6b shows that the minimum efficiency of power dissipation (η) can be obtained when the deformation temperature is low and the strain rate is high. η increases with temperature increasing or strain rate decreasing. Generally, the efficiency (of power dissipation) values associated with DRX are η

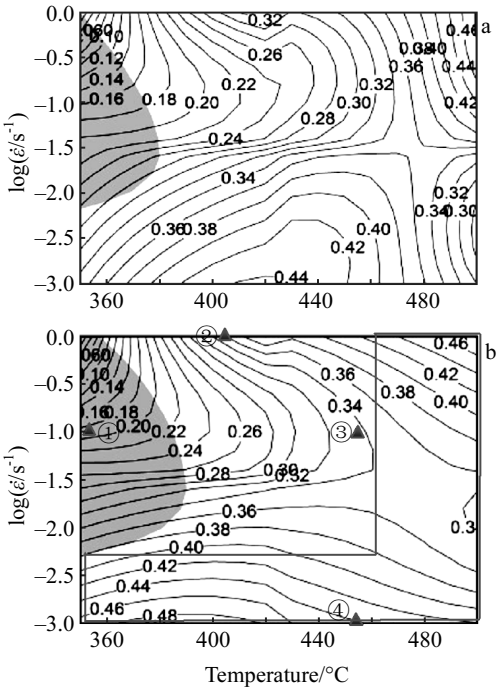

Fig.6 Processing maps of as-homogenized Mg-Gd-Y-Zn-Mn alloy under strains of 0.6 (a) and 1.2 (b)

>35%[18]. Therefore, a material that is deformed in a domain with a high η has good workability. However, a higher η does not necessarily mean better workability because flow instabilities may occur owing to shear band, flow localization, crack and so on. Thus, only those deformation temperatures and strain rates corresponding to both the high efficiency and stability domain in the processing map can be considered as the optimum candidates of hot working parameters.

The instability map describes the variation in the instability parameter with change in temperature and strain rate, where the shaded area parameter represents the domain of the unstable flow. In this study, unstable flow occurs at low temperature and high strain rate, as shown in Fig.6b. Based on the discussion above, the optimum processing conditions for as-homogenized Mg-Gd-Y-Zn-Mn alloy are in the temperature range of 460~500 °C and the strain rate range of 0.001 to 1 s^{-1} or in the temperature range of 350~500 °C and the strain rate range of 0.001 to 0.005 s^{-1}, which is the region in the red box as shown in Fig.6b.

To further verify the correctness of the processing map, the corresponding deformation microstructures should be observed. Fig.7 shows the microstructures of the samples of as-homogenized Mg-Gd-Y-Zn-Mn alloy deformed to a strain of 1.2 under different combinations of strain rate and temperature. The deformation conditions where the microstructural observations were made are marked ①, ②, ③ and ④ on the processing map shown in Fig.6b. The subsequent analysis is about microstructures with various power dissipation values. First, in the unstable regions (①), the microstructure containing localized shear bands across coarse grains is shown in Fig.7a. This microstructure is typical in the instability domain. Second, localized shear bands and apparent DRX are not observed in Fig.7b. The inhibition of the lamellar LPSO prevents the apparent DRX even though the alloy is deformed to a large extent. In addition, η of the microstructure in Fig.7b is 28%, which is between 0 and 35%. Thus, the microstructure has no localized shear bands, and the apparent DRX ($\eta \geq 35\%$) is not observed. Meanwhile, the lamellar phase bend heavily after the severe plastic compression. Third, Fig.7c shows that with $\eta = 34\%$, a small percentage of DRX grains is found, and these grains form along the prior coarse grain boundaries, resulting in a "necklace" structure. The corresponding mechanical properties could be predicted not to be good because of the partial DRX. Fourth, a large percentage of DRX grains occur even though a few coarse grains remain shown in Fig.7d. η here is 45%, nearly approaching the maximum efficiency of power dissipation ($\eta = 48\%$) in the processing map.

To examine the SEM images of the microstructures of the alloy deformed under different conditions in detail, the cracks are clearly observed in the interface between the matrix and LPSO phases in Fig.8a. As mentioned above, the microstructure of Fig.8a is in the instability region, so cracks easily occur. Fig.8b shows the SEM image of the typical microstructure in the safety region, in which a large percentage of DRX grains, and the deformation of LPSO can beclearly observed. During the hot compression, the LPSO phase is significantly changed, resulting in changes in orientation and distortion, as marked with the red circle in Fig.8b. Compared with other conventional magnesium alloys, the formation of deformation kinks in the LPSO phase is considered to be an important mechanism working behind the

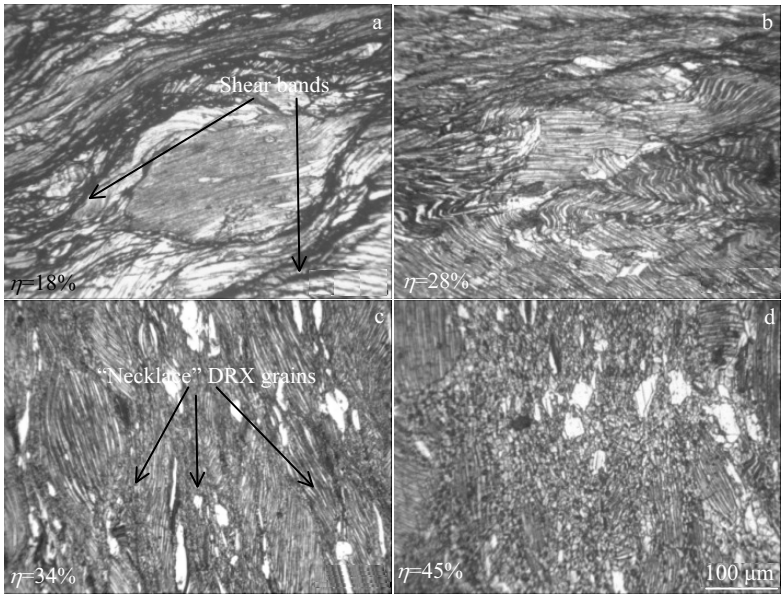

Fig.7 Optical microstructures of the samples with various η values under different compression conditions: (a) 350 °C, 0.1 s^{-1}; (b) 400 °C, 1 s^{-1}; (c) 450 °C, 0.1 s^{-1}; (d) 450 °C, 0.001 s^{-1}

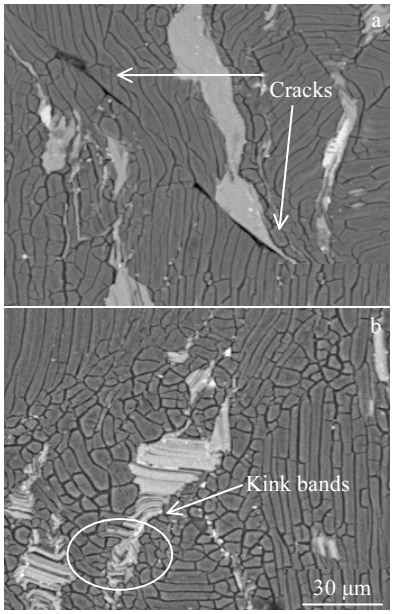

Fig.8 SEM images of the samples under different compression conditions: (a) 350 °C, 0.1 s^{-1} and (b) 450 °C, 0.001 s^{-1}

enhanced ductility and strength of the alloy. Kinking, was observed by J. K. Kim[19], is an essential deformation mechanism to generate homogenous strain in crystals, contributing the ductility of the alloy. N. Tahreen et al.[6] studied the characterization of the hot deformation behavior of an extruded Mg-Zn-Mn-Y alloy containing MgZnY LPSO phase. They schematically described the phenomena of the kink band deformation and pointed out that the flood of dislocations having opposite signs moves along the basal plane of LPSO phase, thereby introducing deformation kink. The mechanism has also been reported and explained by other researchers[20, 21].

In the present study, Mg-Gd-Y-Zn-Mn alloys consist of MgZnY and MgGdZn LPSO phases. The MgZnY LPSO phase could be formed during solidification. However, MgGdZn LPSO phases do not exist in the as-cast ingots, which could be formed during heat treatment (540 °C/4 h, cooled in a furnace). The main composition of the gray bulk LPSO phase at the grain boundary was $Mg_{12}ZnY$, whereas the lamellar LPSO phase that precipitated in the grain was mainly $Mg_{12}ZnGd$ [22]. The two kinds of LPSO phases have the same structure. Therefore, the deformation mechanism of the gray bulk LPSO phase in the as-homogenized Mg-Gd-Y-Zn-Mn alloy is the same as that in the extruded Mg-Zn-Y reported by N. Tahreen.

3 Conclusions

1) The activation energy of the as-homogenized Mg-Gd-Y-Zn-Mn alloy is obtained to be 260.94 kJ/mol. Compared with pure magnesium, the presence of LPSO phase results in higher activation energy. Based on the hyperbolic since law, the constitutive equation is

$$\dot{\varepsilon} = 6.55\times10^{17}[\sinh(0.008376\sigma)]^{5.40314}\exp(-\frac{260.94}{8.314T})$$

2) Based on the DMM, the processing maps of as-homogenized Mg-Gd-Y-Zn-Mn alloy deformed at strain values of 0.6 and 1.2 were established. According to the maps, the optimum processing conditions for as-homogenized Mg-Gd-Y-Zn-Mn alloy are in the temperature range of 460~500 °C and the strain rate range of 0.001 to 1 s^{-1} or in the temperature range of 350~500 °C and the strain rate range of 0.001 to 0.005 s^{-1}.

3) After being compressed to a large strain, the LPSO phase of the as-homogenized Mg-Gd-Y-Zn-Mn alloy exhibits a high degree of deformability. The kink band is observed in the gray bulk LPSO phase, which is due to the motion of dislocation. Moreover, the lamellar phases become stream-shaped phases after hot deformation.

References

1 Wang J, Meng J, Zhang D *et al*. *Materials Science and Engineering A*[J], 2007, 456(1-2): 78
2 Wang C Y, Wang X J, Chang H *et al*. *Materials Science and Engineering A*[J], 2007, 464(1-2): 52
3 Hu H E, Wang X Y, Deng L. *Materials Science and Technology*[J], 2014, 30(11): 1321
4 Prasad B K, Narayan S P, Modi O P *et al*. *Materials Science & Technology*[J], 2011, 27(11): 1639
5 Li H Z, Wang H J, Li Z *et al*. *Materials Science and Engineering A*[J], 2010, 528(1): 154
6 Tahreen N, Zhang D F, Pan F S *et al*. *Journal of Alloys and Compounds*[J], 2015, 644: 814
7 Honma T, Ohkubo T, Kamado S *et al*. *Acta Materialia*[J], 2007, 55(12): 4137
8 Fang X Y, Yi D Q, Nie J F *et al*. *Journal of Alloys and Compounds*[J], 2009, 470(1-2): 311
9 Wang J, Song P, Huang S *et al*. *Materials Letters*[J], 2013, 93: 415
10 Datta A, Waghmare U V, Ramamurty U. *Acta Materialia*[J], 2008, 56(11): 2531
11 Ryan N D, McQueen H J. *Materials Science and Engineering A*[J], 2002, 322: 43
12 Huang X, Zhang H, Han Y *et al*. *Materials Science and Engineering A*[J], 2010, 527(3): 485
13 Chen Q, Xia X, Yuan B *et al*. *Materials Science and Engineering A*[J], 2014, 593: 38
14 Kwak T Y, Lim H K, Kim W J. *Journal of Alloys and Compounds*[J], 2015, 644: 645
15 Prasad Y V R K, Rao K P. *Materials Science and Engineering A*[J], 2005, 391(1-2): 141
16 Prasad Y V R K, Rao K P, Hort N *et al*. *Materials Science and Engineering A*[J], 2009, 502(1-2): 25
17 Lin Y C, Li L T, Xia Y C *et al*. *Journal of Alloys and*

Compounds[J], 2013, 550: 438

18 Shao Z, Zhu X, Wang R *et al*. *Materials & Design*[J], 2013, 51: 826

19 Kim J K, Sandlöbes S, Raabe D. *Acta Materialia*[J], 2015, 82: 414

20 Shao X H, Yang Z Q, Ma X L. *Acta Materialia*[J], 2010, 58(14): 4760

21 Hagihara K, Yokotani N, Umakoshi Y. *Intermetallics*[J], 2010, 18(2): 267

22 Huang S, Wang J, Hou F *et al*. *Materials Science and Engineering A*[J], 2014, 612: 363

均匀化态 Mg-Gd-Y-Zn-Mn 合金热变形行为及加工图

王敬丰[1,2]，谢飞舟[1]，刘世杰[1]，黄　崧[1]，潘复生[1]

(1. 重庆大学 国家镁合金工程技术研究中心，重庆 400044)

(2. 机械传动国家重点实验室，重庆 400044)

摘　要：通过温度在 350~500 ℃，应变速率在 0.001~1 s^{-1} 的热压缩试验，研究了均匀化态 Mg-Gd-Y-Zn-Mn 合金热变形行为和加工图。采用双曲线模型，建立了本构方程，计算的激活能为 260.94 kJ/mol。基于动态材料模型，绘制了应变量为 0.6，1.2 的均匀化态 Mg-Gd-Y-Zn-Mn 合金的加工图，用于研究材料的热成型性能。应变量为 1.2 的加工图显示适合合金加工的两个安全区域：一个是变形温度 460~500 ℃，应变速率 0.001~1 s^{-1}；另一个是变形温度 350~500 ℃，应变速率 0.001~0.005 s^{-1}。同时，讨论了相应的微观组织演变，重点关注了该合金中长程堆垛有序相（LPSO）的变形机制。

关键词：Mg-Gd-Y-Zn-Mn 合金；热变形；加工图；最佳变形参数；微观组织

作者简介：王敬丰，男，1971 年生，博士，教授，重庆大学材料科学与工程学院，重庆 400044，电话：023-65112153，E-mail: jfwang@cqu.edu.cn